Journal of Himalayan Earth Sciences Volume 52, No. 2, 2019 pp. 83-95

Evaluating susceptibility of the 2005 earthquake produced landslides in Kashmir region, Northern Pakistan

Safeer Ullah Shah[1], Muhammad Shafique[1*], Muhammad Basharat[2], Xiaoqing Chen[3], Ihsan Ullah[4] and Muhammad Jamal Nasir[4]

[1]National Centre of Excellence in Geology, University of Peshawar, Peshawar
[2]Institute of Geology, University of Azad Jammu & Kashmir
[3]Institute of Mountain Hazards and Environment, Chinese Academy of Sciences, Chengdu, China
[4]Department of Geography, University of Peshawar
**Corresponding author's email: shafique@uop.edu.pk*
Submitted: 15/07/2019 Accepted:28/10/2019 Published online:

Abstract

On October 8th, 2005 a devastating earthquake in the Kashmir region has triggered widespread landslides, which were considered the second most important driver of devastation to the natural and man-made environment after the earthquake. Landslides susceptibility assessment is the prerequisite for the landslide management, however, considering the dynamic spatial-temporal distribution of co-seismic landslides, an updated landslide susceptibility assessment is of fundamental importance. This paper has evaluated the earthquake-induced landslides and developed an updated landslide susceptibility map. A detailed inventory of the co-seismic landslides is acquired from the SPOT-5 satellite image and field observations. The developed landslide inventory is subsequently cross analyzed with the ASTER based Digital Elevation Model (DEM) computed topographic parameters (curvature, slope angle, aspect, drainage pattern), geology, human activities and fault lines to investigate their influence on landsldies distribution. The derived correlations were statistically analyzed using a Weight-of-Evidence model to develop the landslide susceptibility map. The accuracy of the developed landslide susceptibility is 74 %. The acquired susceptibility map can be used by the relevant departments for the landslide's mitigation and risk reduction.

Keywords: Remote sensing, Kashmir earthquake, Landsldies, Susceptibility.

1. Introduction

On October 8th, 2005, a destructive Kashmir earthquake hit the northern parts of Pakistan with a measured magnitude of 7.6 Mw (USGS, 2005). Epicenter of the earthquake was situated at ~18 km in the northeast of Muzaffarabad at a 26 Km depth (EERI, 2005). The Kashmir earthquake was the deadliest and most disastrous natural hazard in the history of Pakistan with more than 86,000 fatalities, hundreds of thousands of injuries, displacing 2.5 million people and around 5 billion US$ economic loss (ADB-WB, 2005; Peiris et al., 2006; USGS, 2006). The earthquake also produced and reactivated thousands of widespread landslides (Owen et al., 2008). These co-seismic landslides caused about one thousand of direct deaths and several indirectly by the disruption in the roads network (Petley et al., 2006; Owen et al., 2008).

Rainfall and earthquakes are major drivers for widespread landslides (Keefer, 1984; Ayalew et al., 2011). Moreover, earthquakes also destabilize the slopes which might lead to failure if exposed to successive rainfalls or aftershocks (Yang et al., 2017). Hence, monitoring of the unstable slopes is very essential to identify the future potential landslides, understand their triggering mechanism and accordingly develop updated landslide susceptibility maps (Cui et al., 2011). Landslide susceptibility highlight the areas of different susceptibility levels that are predominantly used for the development and implementation of the landslide hazard mitigation (Shafique et al., 2016). Landslide susceptibility can be evaluated using a heuristic, deterministic and statistical techniques (Saha et al., 2005; Yoshimatsu and Abe, 2006; Sharma and Kumar, 2008). Weights-of-Evidence (WOE) modeling using statistical Bayesian theorem is effectively used for landslide susceptibility assessment (Dahal et al., 2008). The WOE was initially used for potentially available mineral mapping (Bonham-Carter et al., 1989; Bonham-Carter,

1994). Subsequently, it has been extensively used in the fields of geosciences, flowing well mapping, to evaluate the relationship between fault lines and seismic activities, slopes instabilities associated with mines and landslide susceptibility mapping (Carranza and Hale 2002; Cheng, 2004; Süzen and Doyuran, 2004; Ilia and Tsangaratos, 2016).

Remotely sensed imagery and Geographical Information System (GIS) are efficiently applied for landslide susceptibility assessment (Van Westen et al., 2008; Harp et al., 2011; Basharat et al., 2014; Xu et al., 2014). Remote sensing-based generated landslide inventories can be used to assess the influence of landslide causative parameters on the landsldies distribution. Landslide inventory is generally acquired from different sources of remotely sensed data (satellite images), using manual digitization, pixel and object-based digital image classification (Fan et al., 2019). Temporal analysis of sequential satellite imagery can be used effectively to evaluate the spatial-temporal dynamics in the co-seismic landslides, to identify the active landslides and understand their triggering mechanism; and accordingly mitigate their devastating impacts (Yang et al., 2017).

The landslides produced by the 2005 Kashmir earthquake are widely studied (Petley et al., 2006; Sato et al., 2007; Owen et al., 2008; Khattak et al., 2010; Saba et al., 2010; Basharat et al., 2014; Basharat et al., 2016; Shafique et al., 2016). Landslide susceptibility maps are developed by Kamp et al., (2008), and Kamp et al., (2010) for the region, however, the dynamic nature of landslides in the region highlight the need for an updated and more realistic landslide susceptibility map. The aim of this study is to develop a comprehensive landslide inventory, analyze their distribution and develop a landslide susceptibility map.

2. Study area

The study area is comprised of Balakot and Muzaffarabad in Pakistan with a total area of 765 km^2 (Fig. 1). The area was affected severely by the earthquake. Subtropical highland climatic conditions are prevailing in the study area with mean minimum and maximum temperatures vary from 3.2˚-15.9℃ in January and 22.1-36.6˚C in June (WMO, 2007). The average rainfall in the area is varying from 1000 and 2000 mm.yr-1, depending on the strength of the monsoon season (Basharat et al., 2016).

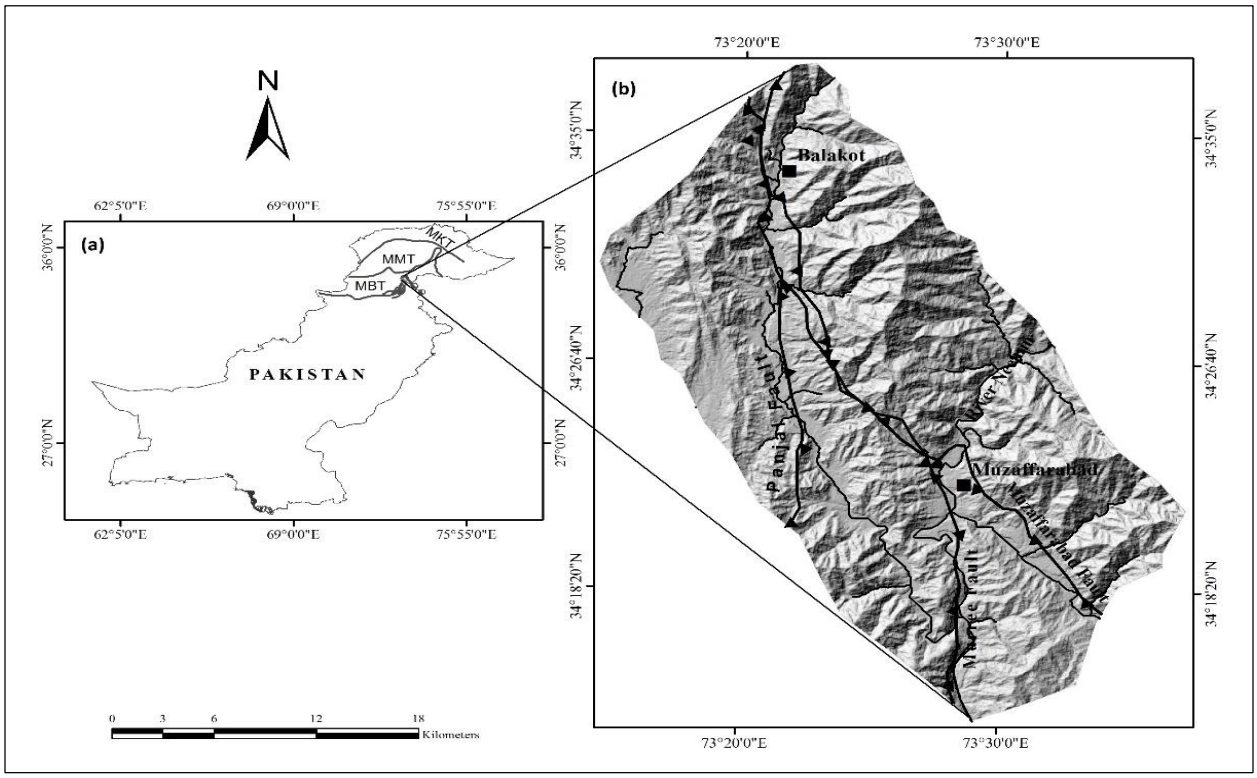

Fig. 1. Location map of the study area showing the topography, rivers, cities and fault network through the study area (b) and in the region (a)

The area has witnessed frequent and devastating landslides which can be attributed to rugged topography, frequency seismic activities, cracked lithology, and human factors. Geologically, the area is comprised of different lithological units (Table 1, Fig. 2) (Hussain et al., 2004; Latif et al., 2008). The occurrence of many faults (Jhelum, Muzaffarabad, MBT, and MBT) and fold structures (Muzaffarabad anticline and Hazara-Kashmir syntaxis) have resulted in these lithologies jointed and fractured. These geological and tectonic conditions are further weakening the mechanical strength of the local lithologies. Moreover, the rough terrain with elevated mountains, steep slopes and deep-cut valleys has aggravated the fragility of these rock formations. The overall terrain is mountainous and elevated more than 4000 m from the average sea level. The landscape of the area is mainly divided in valley floors with an elevation of 600-900 m. The study area is drained by the major rivers including the River Jhelum, River Neelum River, and River Kunhar, forming antecedent valleys (Fig. 1). The river valleys are mainly covered with depositional landforms including river terraces, alluvial fans, and flood plains. The flow of the rivers is fast which also leads to high erosion rates and fluvial incisions with steep slopes and therefore became easy prey for landsliding.

3. Materials and methods

3.1. *Data collection*

The SPOT-5 images of 2.5 m spatial resolution were applied to acquire landslide inventory. The inventory was developed using the visual image interpretation of the acquired images, supported by field observations. The ASTER DEM with a spatial resolution of 30 m was used to derive topographic attributes including curvature, drainage, slope, and aspect. Figure 3 shows a few representative examples of active landslides.

3.2. *Causative factors*

Topographic attributes and geomorphologic features have a great influence on the distribution of landslides (Dahal et al., 2008). Topographic attributes of aspect, slope, and curvature were computed from the ASTER DEM to evaluate their influence on landslides. Terrain slopes located near to the fault lines are usually prone to landslides, and therefore influence the distribution of landslides (Lee, 2005). Buffer zones of 500 m intervals from the fault line were computed to evaluate its impact on the landslides distribution. Undercutting of slopes and the vibrations, related to road construction, uncontrolled blasting, and heavy traffic can eventually lead to slope failures (Das et al., 2012). Road network for the study was extracted from the SPOT-5 (acquired in 2014) satellite image. Buffer zones of 100 m intervals from the road network were prepared. The drainage network is known as one of the causes for landslides, because of its continuous erosion at the slope toe, that eventually leads to landslides (Dahal et al., 2008). The drainage network with a minimum flow accumulation of 25 Km^2, was computed from the ASTER DEM and distance to drainage network was also computed. All these thematic layers were rasterized to 30 m spatial resolution and compared with the inventory of landslide for susceptibility assessment.

Table 1. Geological formations with their lithologies and age in the study area, after Hussain et al., (2004) and Latif et al., (2008). The geological map of the area is given in Figure 2.

Formations	**Lithology**	**Age**
Poorly or unconsolidated alluvium/colluvium deposits	gravels, sand, and clay	Quaternary to recent
Murree Formation	Mudstone, Siltstone, Sandstone, Shale	Miocene
Margala Hill limestone	Limestone	Eocene
Hangu-Patala Formations	Sandstone, shale, limestone,	Paleocene
Panjal Formation	Greeschist (metabasalt) , pelite and marble	Permian
Abbottabad /Muzaffarabad Formation	Dolomite, sandstone, quartzite limestone	Cambrian
Mansehra orthogenesis	Granite, doerite dykes	Cambrian
Tanawal Formation	Quartzite, quartzose Schist	Precambrian
Hazara Formation	Slate, shale, siltstone, limestone	
Salkhala Formation	Pelitic schist, limestone	

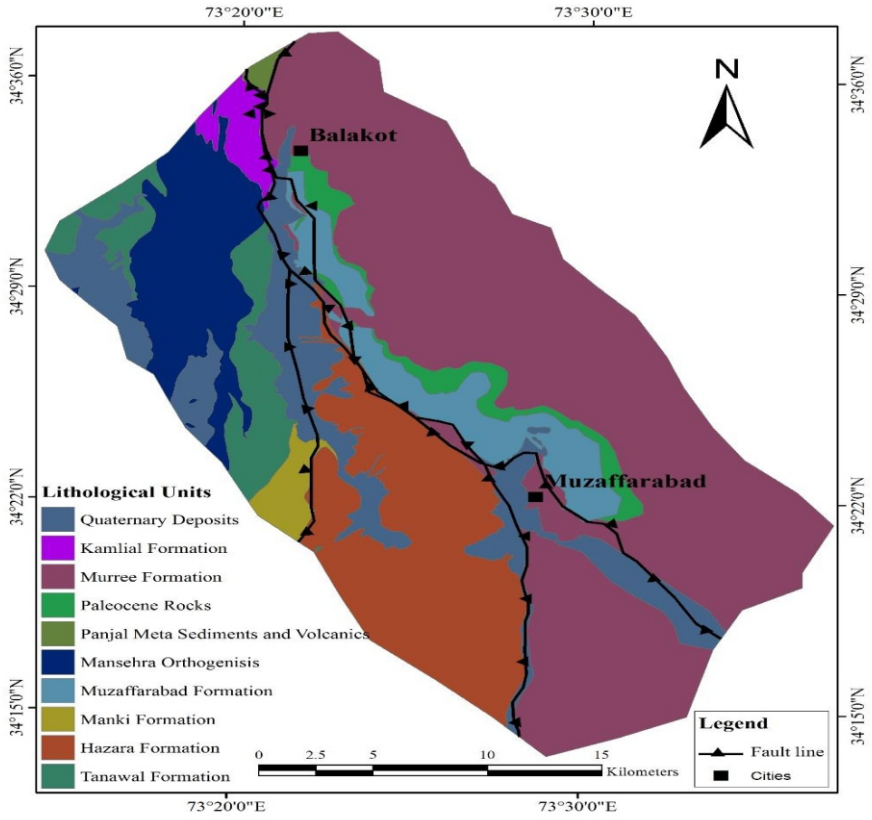

Fig. 2. Spatial distribution of geological formations in the study area, after Hussain et al. (2004) and Latif et al. (2008).

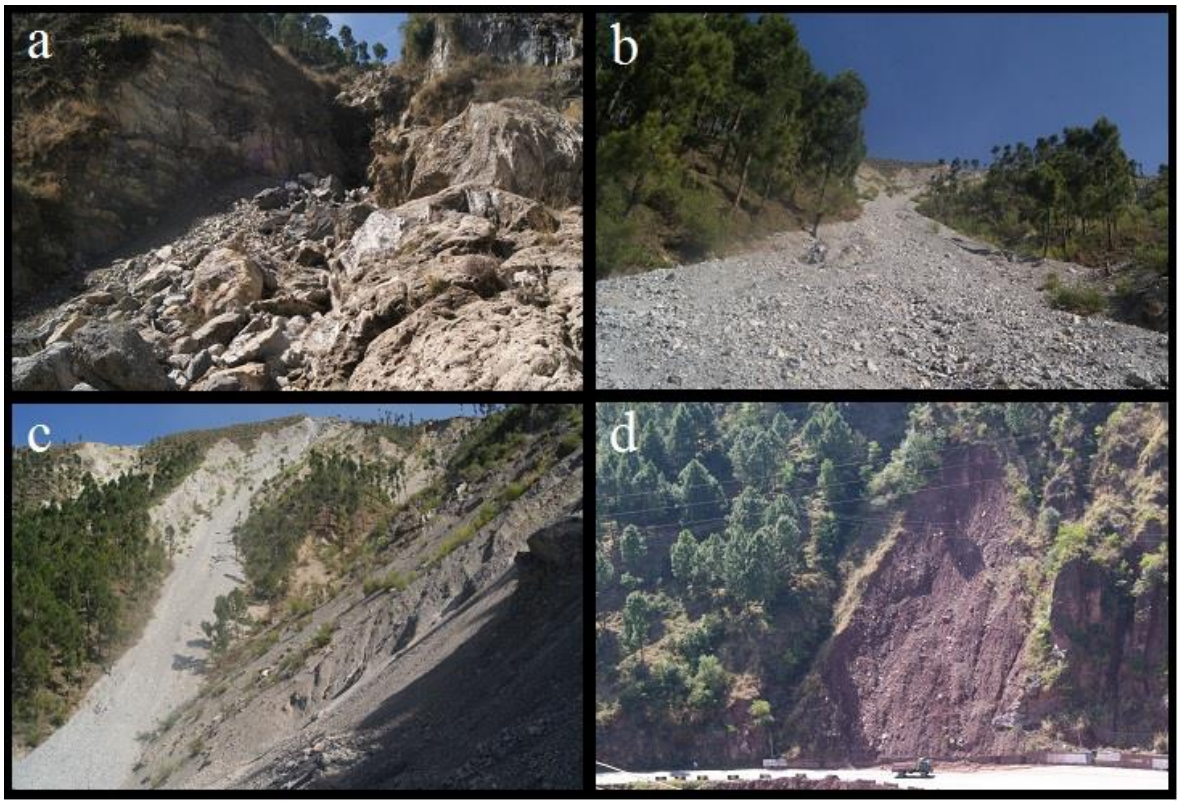

Fig. 3. Illustrative examples of the landslide activity in the study area. (a) rockfall (b) debris flow (c) debris avalanche (d) rotational landslide

3.3. *Weights-of-evidence model*

Weights-of-Evidence modeling is frequently and efficiently applied for landslide susceptibility assessment. Probabilities (Prior and Posterior) are used with enough data to calculate the relative significance of causative factors by statistical means (Bonham-Carter, 1994). This technique computes the weight for each of the selected causative factors, considering their absence or presence of landslides. This technique assumes that the landslides will occur because of the present conditions that contribute to the current or past landslides (Dahal et al., 2008). The basic theme of the model is to calculate the weights of the causative factors (B) on the basis of absence/presence (S) within the given area. The weights for the causative factors are defined as:

$$W^{+} = \ln\left[\frac{P\{B/S\}}{P\{B/\bar{S}\}}\right] \qquad (1)$$

$$W^{-} = \ln\left[\frac{P\{\bar{B}/S\}}{P\{\bar{B}/\bar{S}\}}\right] \qquad (2)$$

Where P is the probability, Ln is the natural log, B is the presence of landslide causative factor, and $\bar{B}$ is the absence of landslide causative factors. S is the presence of landslides and $\bar{S}$ is the absence of landslides.

For each of the causative factors, W^{+} specifies the significance of the existence of the causative factor for the incidence of landslides. If W^{+} is positive, the existence of the causative factor is promising for the incidence of landslides and if W^{+} is negative, it is unfavorable. Similarly, W^{-} is used to determine the significance of the absence of the causative factor. When W^{-} is positive, the absence of a causative factor is promising for the occurrence of the landslide, and when W^{-} is negative, the causative factor is unfavorable. The value of the contrast (C) is the difference between W^{+} and W- and calculated using equation 3.

$$C = W^{+} - W^{-} \qquad (3)$$

4. Results

4.1. *Landslide distribution and inventory map*

On the basis of visual classification of the 2014 satellite image and subsequent field visits, 210 landslides were detected and mapped. The minimum area of the mapped landslides was 0.00065 km^2 and the maximum was 0.681 km^2. The mapped landslides were subsequently classified using the landslide classification system of Varnes (1978). Rockfalls were the dominant landslide type in the area (Fig. 4 and Table 2). In the field, it was observed that the majority of the rockfall happened in the Muzaffarabad Formation comprising of rubbly limestone and dolomites. Similarly, rotational and translational landslides were observed in the Hazara Formation that mainly comprised of shale and slates lithologies.

4.2. *Impacts of causative factors on landslides*

Using equations 4 and 5, the landslide causative factors (Fig. 5 and 2) were compared with the landslide inventory (Fig. 4) and the derived weights (W+, W- and C) for each of the causative factors and classes are given in Table 3. The derived weights are indicating the significance of every causative factor and class. The positive weight gained by the causative factor is favorable for the landslide occurrence and unfavorable in case of negative. The weights that oscillate around zero, indicate little to no impact on the occurrence of landslides.

Table 2. Number of landslides per category, areal coverage and percentage of total landslide affected area

Types	Landslide number	Area (km^2)	Area (%)
Debris avalanche	4	0.144	0.916
Flow slide	4	0.133	0.85
Rockfall	112	9.231	58.65
Slide (Rotational and Translational)	88	6.215	39.5
Topple	2	0.016	0.103

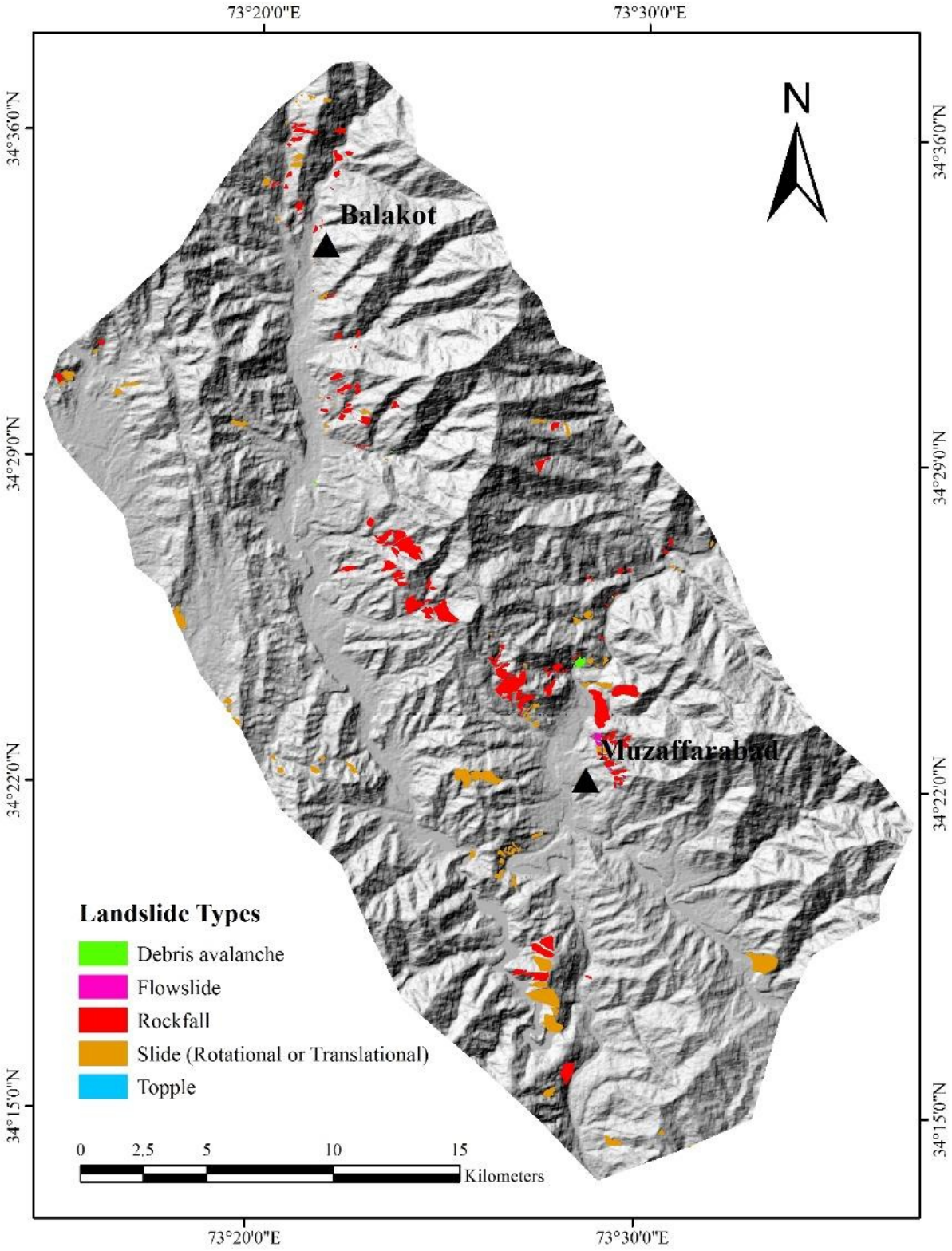

Fig. 4. Spatial distribution of landslides and types in the area based on 2014 satellite image and field observations.

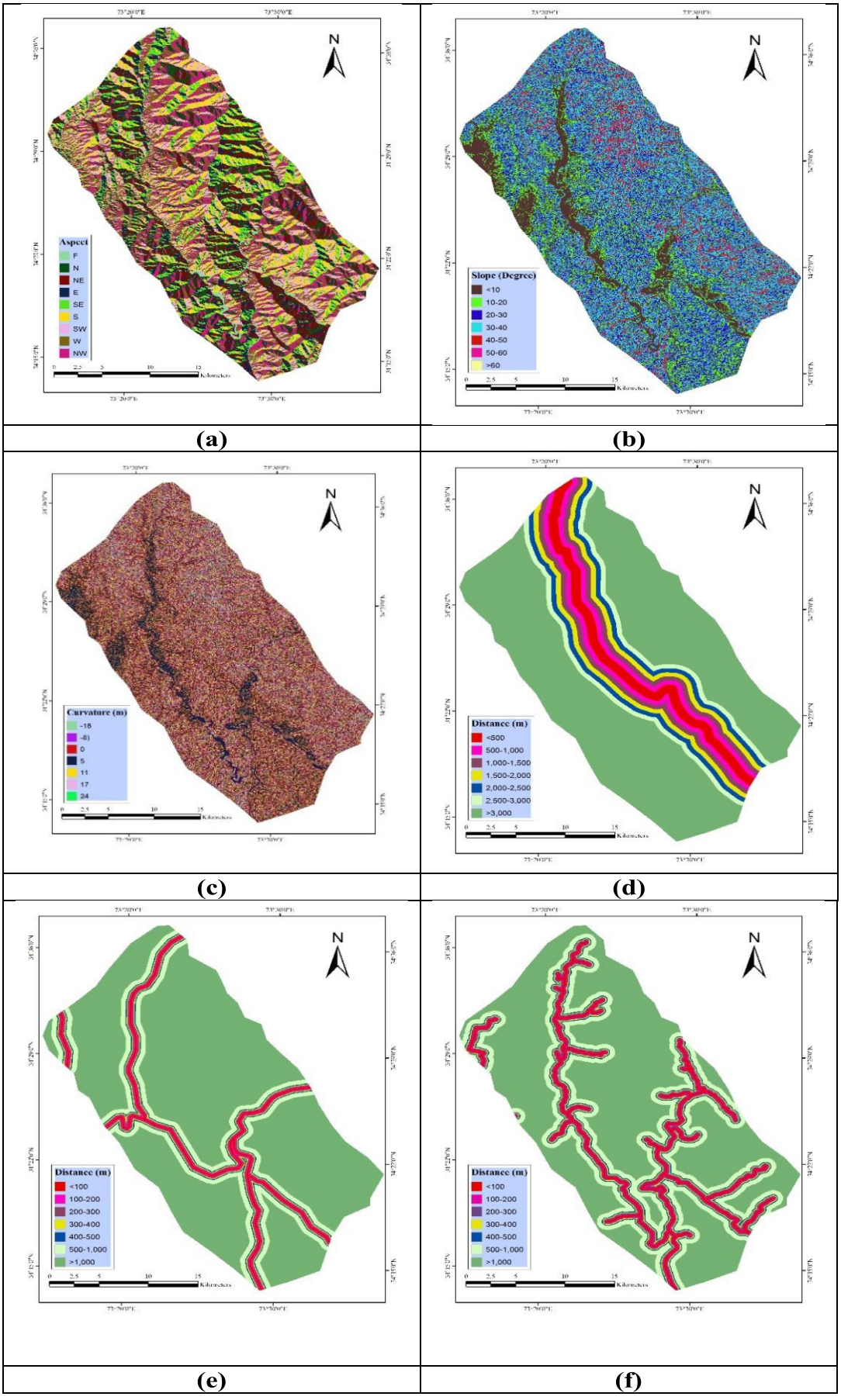

Fig. 5. Thematic data layers used in the study to evaluate their impact on the distribution of landslides, (a) slope, (b) aspect, (c) curvature (d) fault (e) road (f) drainage.

The terrain, facing the west, south-west, and south directions are most prone to landslides (Table 3), which is also observed by Basharat et al., (2014). The terrain with the highest convexity is prone to landslides. The distance of 200-400 m from the drainage network is observed as prone to landslides. The locations in the close neighborhood of the fault line are more prone to landslides. The buffer zone of 1 km around the fault is prone to landslides and further away the landslides are decreasing. A direct correlation of terrain slope with landslide occurrence is observed. Among the topographic attributes, the terrain slope has a substantial impact on the distribution of landslides. Among the geological formations, the maximum number of landslides was hosted by the Muzaffarabad Formation (41.84 %) followed by the Hazara Formation (25 %).

4.3. Landslide susceptibility mapping

The derived weights maps were calculated numerically to acquire the Landslide Susceptibility Index (LSI) map (Fig. 6a) based on the equation 6.

$$LSI = W_f Slope + W_f Geology + W_f Aspect + W_f Curvature + W_f Dist\_drn + W_f Dist\_fault + W_f Dist\_road \quad (6)$$

The LSI map was further classified into four zones using natural break method according to the intensity levels of landslide susceptibility (Fig. 6b). In the derived susceptibility map, a very high landslide susceptibility zone covers 3.01 % of the area. The very high susceptible zones are concentrated along the Muzaffarabad fault, indicating the significant impact of the fault line on the landslides. The high landslide susceptibility zone covers 11.48 % of the total study area and contains 35.85 % of the landslide area. The moderate landslide susceptibility zone covers 67.44 % of the area. The low landslide susceptibility zone covers 18.07 % of the area.

The Success Rate Curve shown in Figure 7, was obtained by calculating the index values of all pixels in the susceptibility map. The overall accuracy achieved by the model is 74% which is a notable agreement between the observed landslides and landslide susceptibility map.

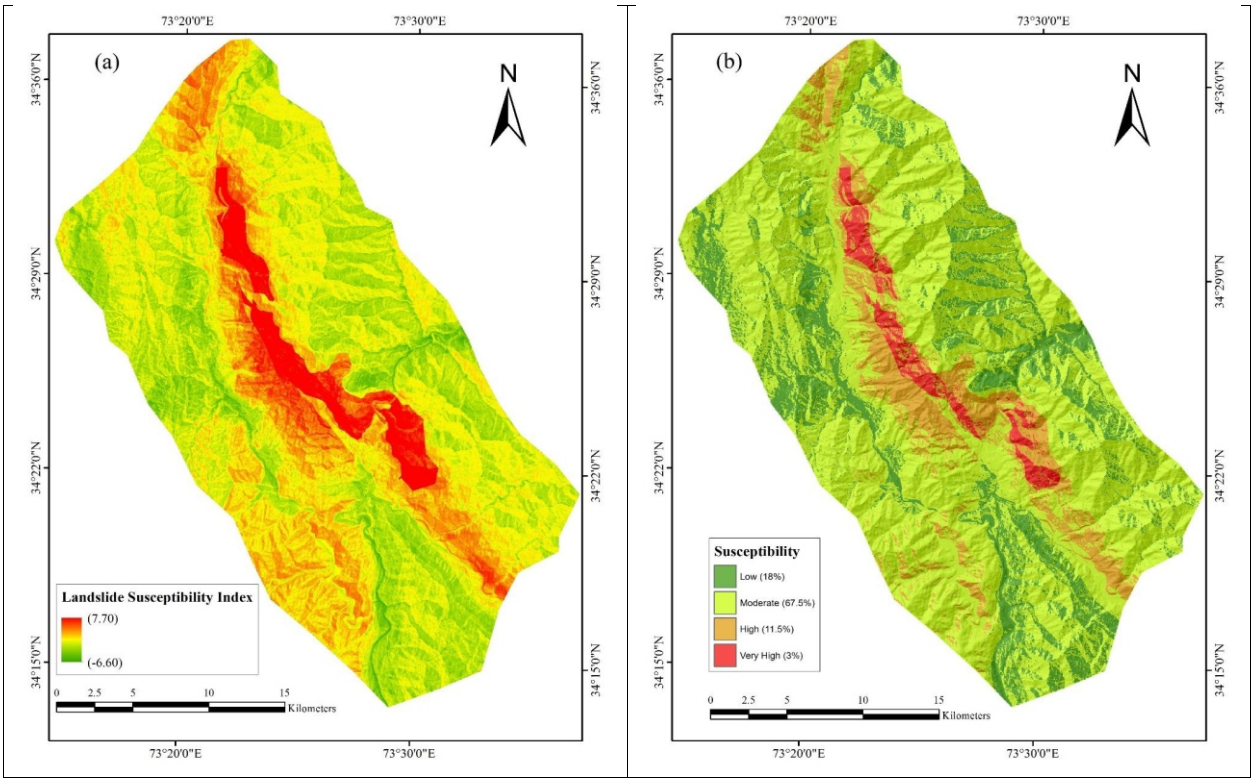

Fig. 6. (a) LSI map (b) and Landslide susceptibility map of the study area.

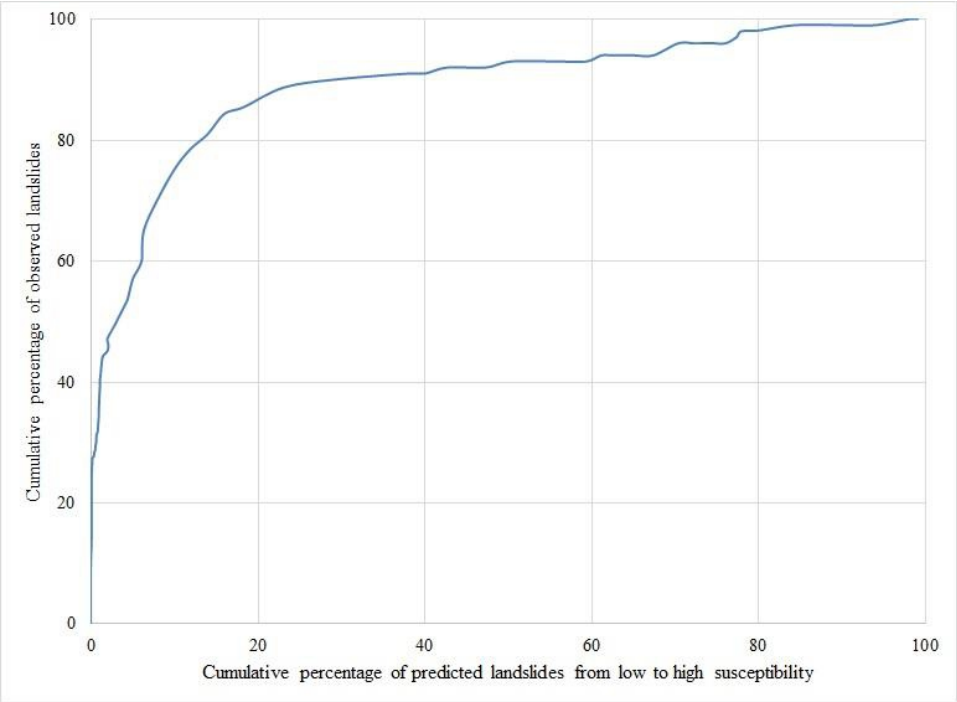

Fig. 7. Success rate curve of the developed landslide susceptibility map.

Table 3. Results of the WOE model for the landslide causative factors selected for study.

Parameter	Class	No of Pixels in a class	% of Pixels in a class	Area (km^2)	No of Landslide pixels in a class	% of Landslide pixels in a class	Area (Km^2)	W+	W-	C
Aspect	F	9534	1.01	7.72	167	0.86	0.14	-0.16	0.00	-0.17
	N	47534	5.03	38.50	328	1.69	0.27	-1.11	0.04	-1.14
	NE	97759	10.35	79.18	771	3.97	0.62	-0.97	0.07	-1.04
	E	111582	11.81	90.38	1249	6.43	1.01	-0.62	0.06	-0.68
	SE	116402	12.32	94.29	1945	10.01	1.58	-0.21	0.03	-0.24
	S	123595	13.08	100.11	3316	17.06	2.69	0.27	-0.05	0.32
	SW	134312	14.21	108.79	4451	22.90	3.61	0.49	-0.11	0.60
	W	139833	14.80	113.26	4639	23.87	3.76	0.49	-0.11	0.61
	NW	115275	12.20	93.37	2145	11.04	1.74	-0.10	0.01	-0.12
	N	49102	5.20	39.77	427	2.20	0.35	-0.87	0.03	-0.90
Curvature	-18	17019	1.80	13.79	533	2.74	0.43	0.43	-0.01	0.44
	-8	79674	8.43	64.54	2208	11.36	1.79	0.31	-0.03	0.34
	0	218155	23.09	176.71	4561	23.46	3.69	0.02	-0.01	0.02
	5	312912	33.11	253.46	5250	27.01	4.25	-0.21	0.09	-0.30
	11	198326	20.99	160.64	3880	19.96	3.14	-0.05	0.01	-0.06
	17	94929	10.05	76.89	2295	11.81	1.86	0.17	-0.02	0.19
	24	23913	2.53	19.37	711	3.66	0.58	0.38	-0.01	0.39
Distance from drainage	<100	44898	4.75	36.37	598	3.08	0.48	-0.44	0.02	-0.46
	100-200	42218	4.47	34.20	1019	5.24	0.83	0.16	-0.01	0.17
	200-300	40625	4.30	32.91	1162	5.98	0.94	0.34	-0.02	0.36
	300-400	39479	4.18	31.98	1128	5.80	0.91	0.34	-0.02	0.35
	400-500	38023	4.02	30.80	1010	5.20	0.82	0.26	-0.01	0.27
	500-1000	174896	18.51	141.67	3996	20.56	3.24	0.11	-0.03	0.13
	>1000	564855	59.78	457.53	10525	54.15	8.53	-0.10	0.13	-0.23

Distance from fault line	<500	57964	6.13	46.95	4291	22.08	3.48	1.34	-0.19	1.53
	500-1000	57078	6.04	46.23	3590	18.47	2.91	1.16	-0.14	1.31
	1000-1500	56081	5.93	45.43	2454	12.62	1.99	0.78	-0.08	0.85
	1500-2000	55198	5.84	44.71	1104	5.68	0.89	-0.03	0.00	-0.03
	2000-2500	54179	5.73	43.88	743	3.82	0.60	-0.41	0.02	-0.43
	2500-3000	53571	5.67	43.39	407	2.09	0.33	-1.01	0.04	-1.05
	>3000	610920	64.65	494.84	6849	35.24	5.55	-0.62	0.62	-1.24
Distance from road	<100	24512	2.59	19.85	321	1.65	0.26	-0.46	0.01	-0.47
	100-200	24146	2.56	19.56	290	1.49	0.23	-0.55	0.01	-0.56
	200-300	23694	2.51	19.19	233	1.20	0.19	-0.75	0.01	-0.76
	300-400	23259	2.46	18.84	260	1.34	0.21	-0.62	0.01	-0.63
	400-500	22709	2.40	18.39	229	1.18	0.19	-0.72	0.01	-0.74
	500-1000	107839	11.41	87.35	1544	7.94	1.25	-0.37	0.04	-0.41
	>1000	718835	76.07	582.25	16561	85.20	13.41	0.12	-0.49	0.60
Slope	<10	125034	13.23	101.28	899	4.62	0.73	-1.06	0.10	-1.16
	10-20	183778	19.45	148.86	2545	13.09	2.06	-0.40	0.08	-0.48
	20-30	273565	28.95	221.59	5497	28.28	4.45	-0.02	0.01	-0.03
	30-40	254614	26.95	206.24	6864	35.31	5.56	0.28	-0.12	0.40
	40-50	98338	10.41	79.65	3299	16.97	2.67	0.50	-0.08	0.58
	50-60	9494	1.00	7.69	322	1.66	0.26	0.51	-0.01	0.52
	>60	105	0.01	0.09	12	0.06	0.01	1.82	0.00	1.82
Geology	Hazara Formation	147473	15.61	119.45	4853	24.97	3.93	0.48	-0.12	0.60
	Manki Formation	13290	1.41	10.76	160	0.82	0.13	-0.54	0.01	-0.55
	Mansehra Orthogenisis	81987	8.68	66.41	585	3.01	0.47	-1.07	0.06	-1.13
	Murree Formation	439262	46.49	355.80	3155	16.23	2.56	-1.07	0.46	-1.53
	Muzaffarabad Formation	57264	6.06	46.38	8210	42.24	6.65	2.08	-0.49	2.57
	Paleocene Rocks	25356	2.68	20.54	274	1.41	0.22	-0.65	0.01	-0.67
	Panjal Meta Sediments and Volcanics	1950	0.21	1.58	27	0.14	0.02	-0.40	0.00	-0.40
	Quaternary Deposits	115704	12.24	93.72	1390	7.15	1.13	-0.55	0.06	-0.60
	Salkhala Formation	15605	1.65	12.64	161	0.83	0.13	-0.70	0.01	-0.71
	Tanol Formation	47097	4.98	38.15	623	3.21	0.50	-0.45	0.02	-0.47

5. Discussion

The SPOT-5 image was effectively used to develop an inventory of the 2005 Kashmir earthquake-triggered landslides. The number and area covered by the mapped earthquake-induced landslides vary from other studies such as Basharat et al., (2014). These differences can be credited to variation in the coverage of the investigated area, time of mapping and resolution of the utilized satellite images (Shafique et al., 2016). Contrary to Sato et al., (2007) and Basharat et al., (2014), landslides were mapped as polygons rather than as points to express the spatial range of triggered landslides. Following Guzzetti et al., (2012), we have mapped the landslide location, spatial extent, type of movement using SPOT-5 imagery and field observations. In the study, after the earthquake images were used to map landslides and therefore the developed inventory might also include the pre-earthquake landslides, as also by Sato et al., (2007) and Basharat et al., (2014). Ideally, pre

and post-earthquake remotely sensed imagery shall be applied, to delineate the landslide activated specifically by the earthquake. The resolution of utilized SPOT-5 images is 2.5 m, and therefore minor landslides are detected that might not be visible in relatively coarse resolution ASTER (Lodhi, 2011) and Landsat images, due to the coarsening and smoothening effect (Shafique et al., 2011).

The landslide causative factors including topography, local geology, and anthropogenic factors have a significant influence on the landslides distribution, which is also detected during the 2008 Wenchuan earthquake (Wang et al., 2009). The distribution of landslides is mainly determined by the distance from the fault that can be partly explained by the earthquake-induced maximum slip rupture of 9.6 m (Pathier et al., 2006). These fault rupture persuaded ground displacement, are mapped as the earthquake-induced landslides, and resulting in the strongest impact on landslides distribution. After the distance from the fault, the terrain slope has the strongest impact on landslides distribution. Among the geological formations, the Muzaffarabad formation is hosting most (41.84%) of the landslides, mainly rockfalls. However, the utilized geological map is mainly displaying the geological formations which are a cluster of different lithologies, and therefore also leads to variation in the derived impact of lithological units on earthquake-induced earthquake-induced landslides, as indicated by different authors (Shafique et al., 2016).

6. Conclusions

Remote sensing data of SPOT-5 with the field observations were effectively applied to prepare an inventory map of the 2005 Kashmir earthquake-triggered landslides. Rockfall was mostly observed in the area. The landslide causative factors including geology, topographic attributes, distance from the road, fault and drainage show considerable influence on the distribution of landslides. The distance from fault and terrain slope has the highest influence on the distribution of landslides in the area. The derived influence of the causative factors on landslide distribution using the weight of evidence modeling is used to develop a landslide susceptibility map. The developed landslide susceptibility map can be used for landslide mitigation and risk reduction.

Acknowledgment

The authors are grateful to the Pakistan Science Foundation project number PSF/NSFC/Earth-KP-UoP(11) and Natural Science Foundation China Grant No.41661144028 for supporting this study.

Author's Contribution

Mr. Safeer Ullah Shah and Muhammad Shafique envisaged the idea and research. Dr. Basharat supported in the field and data analysis. Xiaoqing Chen, Ihsanullah and Jamal Nasir supported in writing the manuscript.

References

ADB-WB, 2005. Preliminary damage and needs assessment, Asian development bank and world bank, Islamabad, Pakistan, 124.

Ayalew, L., Kasahara, M., Yamagishi, H., 2011. The spatial correlation between earthquakes and landslides in Hokkaido (Japan), a GIS-based analysis of the past and the future. Landslides, 8(4), 433-448.

Basharat, M., Rohn, J., Baig, M. S., Khan, M. R., 2014. Spatial distribution analysis of mass movements triggered by the 2005 Kashmir earthquake in the Northeast Himalayas of Pakistan. Geomorphology 206: 203-214.

Basharat, M., Shah, H. R., Hameed, N., 2016. Landslide susceptibility mapping using GIS and weighted overlay method: A case study from NW Himalayas, Pakistan. Arabian Journal of Geosciences, 9(4), 1-19.

Bonham-Carter, G. F., 1994. Geographic Information Systems for Geoscientists, Modeling with GIS, Oxford: Pergamon press.

Bonham-Carter, G. F., Agterberg, F. P., Wright, D. F., 1989. Weights of evidence modelling: a new approach to mapping mineral potential. Statistical applications in the earth science. Geological Survey of Canada, Paper 9, (89), 171–183.

Carranza, E. J. M., Hale, M., 2002. Spatial

association of mineral occurrences and curvilinear geological features. Mathematical Geology, 34(2), 203-221.

Cheng, Q., 2004. Application of weights of evidence method for assessment of flowing wells in the Greater Toronto area, Canada. Natural Resources Research, 13(2), 77-86.

Cui, P., Chen, X.-Q., Zhu, Y. Y., Su, F. H., Wei, F. Q., Han, Y. S., Liu, H. J., Zhuang, J. Q., 2011. The Wenchuan Earthquake (May 12, 2008), Sichuan Province, China, and resulting geohazards. Natural Hazards, 56(1), 19-36.

Dahal, R. K., Hasegawa, S., Nonomura, A., Yamanaka, M., Dhakal S., Paudyal, P., 2008. Predictive modelling of rainfall-induced landslide hazard in the Lesser Himalaya of Nepal based on weights-of-evidence. Geomorphology, 102(3-4), 496-510.

Das, I., Stein, A., Kerle, N., Dadhwal, V. K., 2012. Landslide susceptibility mapping along road corridors in the Indian Himalayas using Bayesian logistic regression models. Geomorphology, 179, 116-125.

Earthquake Engineering Research Institute (EERI), 2005. First report on the Kashmir Earthquake of October 8, 2005.

Fan, X., Scaringi, G., Korup, O., West, A. J., Van Westen, C. J., Tanyas, H., Hovius, N., Hales, T. C., Jibson, R. W., Allstadt, K. E., Zhang, L., Evans, S. G., Xu, C., Li, G., Pei, X., Xu, Q., Huang, R., 2019. Earthquake-induced chains of geologic hazards: patterns, mechanisms, and impacts. Reviews of Geophysics.

Guzzetti, F., Mondini, A. C., Cardinali, M., Fiorucci, F., Santangelo, M., Chang, K. T, 2012. Landslide inventory maps: New tools for an old problem. Earth-Science Reviews, 112, 42-66.

Harp, E. L., Keefer, D. K., Sato, H. P., Yagi, H., 2011. Landslide inventories: the essential part of seismic landslide hazard analyses. Engineering Geology, 122(1), 9-21.

Hussain, A., Mughal, N., Haq, I., Latif, A., 2004. Geological map of the Gari Habib Ullah area, district Mansehra and parts of Muzaffarabad District, AJK. Geological Map Series. Islamabad-Pakistan, Geological Survey of Pakistan.

Ilia, I., Tsangaratos, P., 2016. Applying weight of evidence method and sensitivity analysis to produce a landslide susceptibility map. Landslides, 13(2), 379-397.

Keefer, D. K., 1984. Landslides caused by earthquakes. Geological Society of America Bulletin, 95(4), 406-421.

Kamp, U., Khattak, G. A., Owen, L. A., Harp, E. L., 2010. Evolution of earthquake-triggered landslides in the Kashmir Himalaya, northern Pakistan. Geomorphology, 115(1), 102-108.

Kamp, U., Owen, L. A., Khattak, G. A., Harp, E. L., Keefer, D. K., Bauer, M. A., 2008. Landslides triggered by the 8 October 2005 Kashmir earthquake. Geomorphology, 94(1-2), 1-9.

Latif, A., Afridi, A. G. K., Majid, A. N., 2008. Geological map of the Balakot quadrangle (Earthquake affected area), District Mansehra, NWFP, Pakistan. Geological Map Series. Islamabad-Pakistan, Geological Survey of Pakistan.

Lee, S., 2005. Application of logistic regression model and its validation for landslide susceptibility mapping using GIS and remote sensing data. International Journal of Remote Sensing, 26(7), 1477-1491.

Lodhi, M. A., 2011. Earthquake-induced landslide mapping in the western Himalayas using medium resolution ASTER imagery. International Journal of Remote Sensing, 32(19), 5331-5346.

Pathier, E., Fielding, E. J., Wright, T. J., Walker, R., Parsons B. E., Hensley, S., 2006. Displacement field and slip distribution of the 2005 Kashmir earthquake from SAR imagery. Geophysical research letters 33(20): n/a-n/a.

Peiris, N., Rossetto, T., Burton, P., Mahmood, S., 2006. EEFIT mission: October 8, 2005 Kashmir earthquake. Published Report, The institution of structural engineers, London.

Petley, D., Dunning, S., Rosser, N., Kausar, A. B., 2006. Incipient landslides in the Jhelum Valley, Pakistan following the 8th October 2005 earthquake. Disaster Mitigation of Debris Flows, Slope Failures and Landslides, 47-55.

Saba, S. B., Van der Meijde, M., Van der Werff, H., 2010. Spatiotemporal landslide

detection for the 2005 Kashmir earthquake region. Geomorphology, 124(1–2), 17-25.

Saha, A. K., Gupta, R. P., Sarkar, I., Arora, M. K., Csaplovics, E., 2005. An approach for GIS-based statistical landslide susceptibility zonation—with a case study in the Himalayas. Landslides, 2(1), 61-69.

Sato, H. P., Hasegawa, H., Fujiwara, S., Tobita, M., Koarai, M., Une H., Iwahashi, J., 2007. Interpretation of landslide distribution triggered by the 2005 Northern Pakistan earthquake using SPOT 5 imagery. Landslides, 4(2), 113-122.

Shafique, M., Van der Meijde, M., Kerle, N., Van der Meer, F., 2011. Impact of DEM source and resolution on topographic seismic amplification. International Journal of Applied Earth Observation And Geoinformation, 13(3), 420-427.

Shafique, M., Van der Meijde, M., Khan, M. A., 2016. A review of the 2005 Kashmir earthquake-induced landslides; from a remote sensing prospective. Journal of Asian Earth Sciences, 118, 68-80.

Sharma, M., Kumar, R., 2008. GIS-based landslide hazard zonation: a case study from the Parwanoo area, Lesser and Outer Himalaya, HP, India. Bulletin of Engineering Geology and the Environment, 67(1), 129-137.

Süzen, M. L., Doyuran, V., 2004. Data driven bivariate landslide susceptibility assessment using geographical information systems: a method and application to Asarsuyu catchment, Turkey. Engineering Geology, 71(3–4), 303-321.

United States Geological Service (USGS), 2005. Magnitude 7.6 - Pakistan. Retrieved 29 October 2010, from http://earthquake.usgs.gov/earthquakes/eqinthenews/2005/usdyae/.

United States Geological Service (USGS), 2006. Magnitude 7.6- Pakistan earthquake 2005 summary, 1-2.

Van Westen, C. J., Castellanos, E., Kuriakose, S. L., 2008. Spatial data for landslide susceptibility, hazard, and vulnerability assessment: An overview. Engineering geology, 102(3), 112-131.

Varnes, D. J., 1978. Slope movement types and processes. Transportation Research Board Special Report(176).

Wang, F., Cheng, Q., Highland, L., Miyajima, M., Wang, H., Yan, C., 2009. Preliminary investigation of some large landslides triggered by the 2008 Wenchuan earthquake, Sichuan Province, China. Landslides, 6(1), 47-54.

World Meteorological Organization (WMO), 2007. Pakistan.

Xu, C., Xu, X., Yao, X., Dai, F., 2014. Three (nearly) complete inventories of landslides triggered by the May 12, 2008 Wenchuan Mw 7.9 earthquake of China and their spatial distribution statistical analysis. Landslides, 11(3), 441-461.

Yang, W., Qi, W., Wang, M., Zhang, J., Zhang, Y., 2017. Spatial and temporal analyses of post-seismic landslide changes near the epicentre of the Wenchuan earthquake. Geomorphology, 276, 8-15.

Yoshimatsu, H., Abe, S., 2006. A review of landslide hazards in Japan and assessment of their susceptibility using an analytical hierarchic process (AHP) method. Landslides, 3(2), 149-158.